FEATURE SELECTION IN PROTON MAGNETIC RESONANCE SPECTROSCOPY DATA OF BRAIN TUMORS

Félix Fernando González-Navarro(1), Lluís A. Belanche-Muñoz(2)

(1) Instituto de Ingeniería
Universidad Autónoma de Baja California
Mexicali, Mexico, fgonzalez@lsi.upc.edu

(2) Dept. de Llenguatges i Sistemes Informàtics
Universitat Politècnica de Catalunya
Barcelona, Spain, belanche@lsi.upc.edu

Keywords: Cancer research, Feature Selection, Classification.

Abstract. In cancer diagnosis, classification of the different tumor types is of great importance. An accurate prediction of different tumor types provides better treatment and may minimize the negative impact of incorrectly targeted toxic or aggressive treatments. Moreover, the correct prediction of cancer types using non-invasive information –e.g. ^{1}H-MRS data– could avoid patients to suffer collateral problems derived from exploration techniques that require surgery. A Feature Selection Algorithm specially designed to be use in ^{1}H-MRS Proton Magnetic Resonance Spectroscopy data of brain tumors is presented. It takes advantage of a highly distinctive aspect in this data: some metabolite levels are notoriously different between types of tumors. Experimental readings on an international dataset show highly competitive models in terms of accuracy, complexity and medical interpretability.

1 Introduction

Proton (or Hydrogen) Magnetic Resonance Spectroscopy (^{1}H-MRS) has been used extensively in biochemistry for *in vitro* chemical analysis of small samples for several years. As a technique for *in vivo* sampling of biological tissue, it provides a quantified biochemical fingerprint of metabolite concentrations [1]. ^{1}H-MRS data has the appearance of a plot of peaks along the x-axis, with the peak position depending on the resonant frequency of the associated metabolite [2]. An example of a ^{1}H-MRS dataset is shown in Fig. 1.

Nowadays, ^{1}H-MRS has been proven its value as a powerful tool in the clinical assessment of several pathologic conditions -e.g. epilepsy, multiple sclerosis, cancer– and specially in neurological affections [3, 4]. Framed as a minimal invasive technique, its application in brain tumor oncological diagnosis carries tremendous benefits to patients, relieving them from complicated surgical procedures and minimizing trauma to normal tissue surrounding the particular lesion or other vital elements.

The use of systematic approaches based on ^{1}H-MRS data for the diagnosis and grading of adult brain tumors is subject of an extensive scientific research. One of these growing approaches takes as backbone well-established machine learning techniques to develop predictive models able to discern between several classes of brain tumors [5, 6, 7]. This particular task is quite challenging, mainly because of the high dimensionality and relatively low number of observations. Therefore, the use of *dimensionality reduction* (and, in particular, feature selection) methods becomes an option in order to present low complexity and interpretable models to oncologists.

In this study, an *ad hoc* feature selection (FS) algorithm is used to generate relevant subsets of spectral frequencies (considered as features). The developed algorithm takes

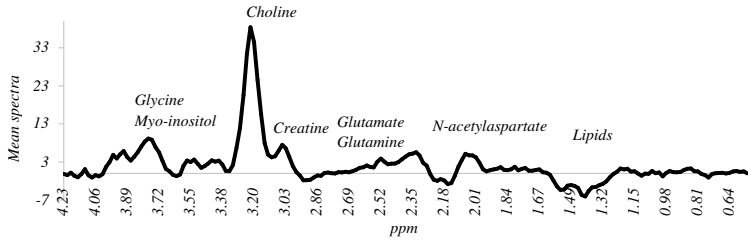

Figure 1: An example of a long time of echo ^{1}H-MRS dataset. Some of the metabolites visible in this kind of spectrum are the Choline, which is a combination of multiple metabolites and is elevated in all brain tumors; the Creatine, a marker of oxidative metabolism of cells; the N-acetylaspartate, a neuronal density marker; the Lipids, seen in condition of necrosis.

advantage of a distinctive aspect shown in typical ^{1}H-MRS readings: some metabolite levels are quite different between types of tumors. Bootstrap resampling is used to reduce sampling variability and obtain more stable readings. We report experimental work in which a small subset of frequencies is able to offer a highly accurate predictive model (a linear classifier). The proposed solution is also discussed in terms of visual appearance and interpretation of the obtained metabolites.

2 Literature review

First attempts using ^{1}H-MRS data in assessing human brain tumors *in vivo* are back to [3]. It was found that spectra differ significantly from normal brain spectra and between tumors by detecting the presence/absence of different metabolites. Even though no machine learning (ML) analysis of spectra was done in establishing these differences, it was concluded that ^{1}H-MRS spectroscopy may help to differentiate tumors for diagnostic and therapeutic purposes, limiting the need for invasive and risky diagnostic procedures such as biopsies.

At this point, ML techniques arise in order to *automate* the classification tasks. Artificial neural networks (e.g. [8, 9]) and linear discriminant analysis (LDA) (e.g. [5, 10]) are commonly used methods. Later studies perform dimensionality reduction, either considering the *peak* signals, ratios between peak signals or *feature extraction* based in principal component analysis or independent component analysis [11, 12, 13]. First studies in performing an explicit feature selection process have used simple well-known search algorithms to select subset of spectral points, such as *forward selection* [14], the Fisher criterion or the Relief feature weighing algorithm [15]. More recent works in FS properly speaking are found in [7, 16, 17, 18], which address a multi-class problem on the same dataset analyzed in this work. The dominant techniques are single-layer neural networks or classical feature selection search algorithms wrapping several classifiers, among which LDA usually yields the best predictive models.

3 Class-Separability Feature Selection

It is known that metabolites (spectral points) in ^{1}H-MRS data present notorious differences among tumors. For example, theoretically, meningiomas do not contain N-acetyl aspartate (NAA) and present the choline (CHO) elevated (up to 300 times the normal reading). Metastases present a moderate reduction in NAA and a decreased creatine (CR) signal. Lipid levels located at 1.3 ppm are mainly arisen in high-grade brain malignancies. These *fingerprints* that distinguish each tumor could lead us to try to establish a measure of physical distance between kinds of tumors that expresses the separability between classes. A very simple choice is taken in this study for this measure: the distance (absolute difference) between the *median* profiles across the different pairs of classes (tumour types).

Taking as primary data a bootstrap distribution, averaged estimations of such distances from the original ^{1}H-MRS data can be computed. The bootstrap distribution of

these values offers other quantities of interest (such as the variance), but these are not used here. The median is used (instead of the mean) with the goal of reducing the influence of possible abnormally high (or low) profiles. If used, these profiles could signal a fake high separability.

The separability degree of metabolites with respect to each tumor is then assessed by the cumulative differences between pairs of elements –i.e. between tumors– thereby obtaining a new feature vector based on distances. It is hypothesized that the direction that best separates tumors taking as basis the metabolites that present abnormal values is partly expressed in this vector.

Algorithm 1: $CSFS$ Class Separability Feature Selection

input : set of bootstrap resamples $S_1, \ldots, S_B$; $\mathcal{L}$ classifier
output: BSS: Best Spectral Subset
1 **foreach** *sample* $b \in \{1, \ldots, B\}$ **do**
2 **foreach** *spectral point* s **do**
3 **foreach** *class* c **do**
4 $m[b, s, c] \leftarrow$ median of spectral point s for class c in S_b
$\bar{m}[s, c] = \frac{1}{B} \sum_{b=1}^{B} m[b, s, c]$
5
6 **foreach** *spectral point* s **do**
7 **foreach** *pair of different classes* (c_i, c_j) **do**
8 $DS[s] \leftarrow DS[s] + |\bar{m}[s, i] - \bar{m}[s, j]|$
9 Sort DS in decreasing order
10 $BSS \leftarrow \varnothing$
11 $Jbest \leftarrow 0$
12 **repeat**
13 ***Forward Stage***
14 **for** $i \in \{1, \ldots, |DS|\}$ **do**
15 **foreach** $sample\ b \in \{1, \ldots, B\}$ **do**
16 $J[b] \leftarrow \mathcal{L}(S_b, S \setminus S_b, BSS \cup \{DS[i]\})$
$\bar{J} \leftarrow \frac{1}{B} \sum_{b=1}^{B} J[b]$
17
18 **if** $\bar{J} > Jbest$ **then**
19 $Jbest \leftarrow \bar{J}$
20 $BSS \leftarrow BSS \cup DS[i]$
21 ***Backward Stage***
22 **repeat**
23 **for** $j \in \{1, \ldots, |BSS|\}$ **do**
24 **foreach** $sample\ b \in B$ **do**
25 $J[b] \leftarrow \mathcal{L}(S_b, S \setminus S_b, BSS \setminus \{BSS[j]\})$
$\bar{J} \leftarrow \frac{1}{B} \sum_{b=1}^{B} J[b]$
26
27 **if** $\bar{J} \geq Jbest$ **then**
28 $Jbest \leftarrow \bar{J}$
29 $BSS \leftarrow BSS \setminus \{BSS[j]\}$
30 **until** *no more Backward improvement*
31 **until** *no more Forward or Backward improvement*

To capture the aforementioned behavior, the CSFS algorithm (which briefs for *Class-Separability Feature Selection*) is designed and outlined in Algorithm 1. Taking as primary data the bootstrap distribution from the original ^{1}H-MRS data, stable distance estimations are computed, and a centroid $\bar{m}$ for every spectral point within each tumor is computed (lines 1-5) and a vector of centroids is generated by averaging them over the B bootstrap samples. In order to asses the separability degree of metabolites with respect to each tumor, the cumulative difference between pairs of elements –i.e. between tumors– is computed (lines 7-9), obtaining a new feature vector based on distances named DS (sorted in decreasing order in line 9). Hence, the CSFS Algorithm takes advantage of abnormal presence of certain metabolites that allows to identify specific tumors. As a consequence, its operation is guided by the ones that present a higher

separability degree in a ranked list.

Once this evaluation is complete, a combined Forward-Backward search strategy is implemented, fed by the DS vector as follows: a Forward step is given taking the first element in the ranked list DS (lines 13-20) and its average performance is evaluated against the bootstrap resamples via a user-defined classifier $\mathcal{L}$. Taking into account that the ^{1}H-MRS data could be considered as a spatial series, in the sense that spectral points are ordered in the metabolic spectrum, it is likely that contiguous spectral points offer similar separability values and hence are found indexed in consecutive positions in DS. For instance, the Creatine peak, located at 3.03 ppm in the spectrum will have a separability value similar to the 3.01 ppm spectral point, which *almost* defines the same metabolite. In order to avoid the inclusion of redundant features, a Backward stage takes place right after every single Forward stage, with the difference that this latter process is executed as much as necessary, and until no improvement is achieved (lines 21-30).

4 Experimental work

In this section, the experimental conditions are outlined. The ^{1}H-MRS dataset employed is described jointly with the brain pathologies involved. Several well known classifiers are used to measure the subsets performance as long as statistical tests to asses uncertainty about comparisons between models.

4.1 *Datasets*

An essential variable in the acquisition of ^{1}H-MRS spectra is the choice of echo time. With short times of echo (around 20 ms), larger numbers of metabolites are detected (myoinositol, glutamate, glutamine), but it is more likely that peak superimposition will occur, causing difficulty in spectroscopic curve interpretation. By using long times of echo (more than 135 ms), most metabolites in the brain are lost (except that of choline, creatine, NAA and lactate), but with better definition of peaks, thereby facilitating graphic analysis[19]. There are a few studies comparing the classification potential of the two types of spectra (see e.g. [10], [6]). These works seem to give a slight advantage to using short time of echo information or else suggest a combination of both types of spectra.

The targeted ^{1}H-MRS data is drawn from a database belonging to the *International Network for Pattern Recognition of tumors Using Magnetic Resonance* (INTERPRET). An European research project aimed to develop systematic tools to enable radiologists and other clinicians without special knowledge or expertise to diagnose and grade brain tumors routinely using magnetic resonance spectroscopy [20]. The dataset is constructed by single voxel ^{1}H-MR spectra acquired *in vivo* from brain tumor patients in two configurations: Long Time of Echo (PRESS 135-144 ms), named LTE, and Short Time of Echo (PRESS 30-32 ms), named STE. Brain pathologies that conform both configurations are distributed as following:

- LTE: 195 observations, including 55 meningiomas, 78 glioblastomas, 31 metastases, 20 astrocytomas grade II, 6 oligoastrocytomas grade II and 5 oligodendrogliomas grade II.
- STE: 217 observations, including 58 meningiomas, 86 glioblastomas, 38 metastases, 22 astrocytomas grade II, 6 oligoastrocytomas grade II, and 7 oligodendrogliomas grade II.

Both spectra were grouped into three super-classes: high-grade malignant tumors (metastases and glioblastomas), low-grade gliomas (astrocytomas, oligodendrogliomas and oligoastrocytomas) and meningiomas. A third configuration was prepared in order to explore the discriminative power of the merged LTE and STE data resulting in 195 common observations of the two previous datasets, and labeled as LSTE.

Table 1: CSFS Feature selection results and final performance. The number in square brackets is the final Best Spectral Subset (BSS) size. The right number is the averaged 10x10 CV accuracy in the original (continuous) ^{1}H-MRS datasets.

	NN	LDC	QDC	LR	lSVM	rSVM
LTE	[11] 89.70	[15] 93.51	[9] 89.09	[7] 91.48	[9] 91.82	[10] **93.88**
STE	[8] 92.21	[16] 93.34	[6] 87.40	[8] 90.48	[12] 93.14	[8] **94.48**
LSTE	[17] 96.14	[26] **98.27**	[8] 92.83	[7] 92.07	[14] 94.83	[12] 94.77

Table 2: Spectral points selected in best solutions –see bold faced models in Table 1.

Best model	ppm
LTE-rSVM	3.74, 2.94, 2.54, 2.35, 1.72, 1.61, 1.25, 1.10, 0.72, 0.66
STE-rSVM	3.81, 3.64, 3.51, 3.07, 2.44, 2.43, 2.37, 2.27
LSTE-LDC	L3.81, L3.66, L3.11, L3.07, L2.98, L2.90, L2.75
	L2.69, L2.29, L2.18, L1.86, L1.55, L0.83, L0.62
	S4.19, S3.81, S3.66, S3.53, S3.49, S2.29, S2.25
	S1.32, S1.13, S1.04, S0.70, S0.66

4.2 *Experimental settings*

The original ^{1}H-MRS datasets $S = \{LTE, STE, LSTE\}$ were used to generate $B = 1,000$ bootstrap samples $S_1, \ldots, S_B$ that play the role of *training sets* in the feature selection process: each classifier $\mathcal{L}$ is developed on each S_b resample and its performance is assessed on the test sample $S \setminus S_b$, and *averaged* across the B bootstrap samples. Once the final BSS is obtained, the final performance is assessed using 10 times 10-fold Cross Validation (10x10 CV) using the original (not discretized) ^{1}H-MRS datasets: the *nearest-neighbor* technique (NN), the *Logistic Regression* (LR), a *Linear and Quadratic Discriminant classifier* (LDC, QDC), *Support Vector Machine* with *linear* kernel (lSVM) and parameter *C* (regularization constant) and *Support Vector Machine with* radial *kernel* (rSVM) and parameters *C* and σ^2 (amount of smoothing in the kernel)[1]. The Wilcoxon signed rank test is applied in order to evaluate a possible statistical significance in the performance of the different models.

5 Discussion of the results

In Table 1, the CSFS feature selection process is displayed. Among the classifiers in LTE data, the rSVM yields the best performance, giving a 93.88% of accuracy with only 10 spectral points; quite close comes LDC at second position with a very similar figure at 93.51% accuracy and 15 spectral points. Precisely, the Wilcoxon signed rank test at 95% level (p-value < 0.05) show significant results comparing the rSVM results against all the others, except with LDC (p-value is 0.160). The STE data experiments show exactly the same behavior, but offering higher readings. The rSVM reaches 94.48% with only 8 spectral points; its first place in this data configuration is supported against all the rest (all p-values are lower than 0.002).

The LSTE experiments render the best results in all cases. The best final performance corresponds to LDC with 98.27% of accuracy using 26 spectral points. Wilcoxon's test p-values give statistical confirmation to this competitive model against all the others. The LSTE-LDC model yields one of the best reported values using this data set *with this particular configuration of super-classes* –see, e.g., [16, 6, 11, 12, 21]. Another recent work reports a very similar final performance, claiming a 98.46% accuracy using 5x5 CV resampling (instead of 10x10 CV as in this study) using 18 spectral points by means of a single-layer Perceptron neural network [18]. This is a very attractive solution since it uses a lesser number of spectral points. However, the developed LSTE-LDC solution uses a classifier that requires no parameter tuning in training phase and

[1] C and σ^2 are optimized via a grid search.

is computationally cheaper. It is also interesting to note that both methods (LDC and the neural network) offer *linear* decision boundaries. The spectral points selected in the best solutions are displayed in Table 2 in terms of their ppm values. The final *selected* feature subset of the best LSTE-LDC model as positioned in the whole spectrum is displayed in Fig. 2. In order to better appreciate the solution in its spectral environment, the mean spectra for the three super-classes are added to the plot.

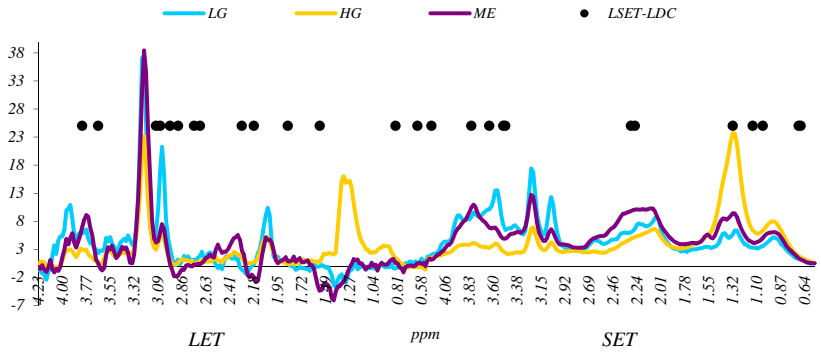

Figure 2: Best Spectral Subset from LSTE-LDC model as positioned in the whole spectrum.

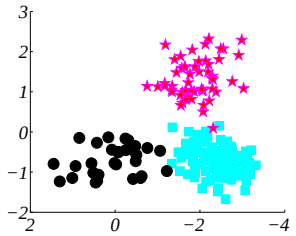

Figure 3: Projection of the dataset (using the final *selected* feature subset of the best LSTE-LDC model) onto the first two eigenvectors of the scatter matrices as coordinate system. Circles represent low-grade *gliomas*; filled squares high-grade *malignant tumors* and stars *meningiomas*.

5.1 *Data visualization*

Data visualization in a low-dimensional space may become extremely important to radiologists, helping them to gain insights into what undoubtedly is a complex domain. We use in this work a method based on the decomposition of the scatter matrix with the property of maximizing the separation between the projections of compact groups of tumor classes –see [24]. Such visualization is illustrated in Fig. 3. These are scatter plots of 3-D projections of the three classes (using the first three eigenvectors of the scatter matrices). It is seen that the three supper-classes are notoriously well separated.

5.2 *Metabolic interpretation*

The metabolites detected and their known biological function are listed in Table 3. It is necessary to clarify that some metabolites posses resonances at different positions in the spectrum –e.g. Threonine or Valine. For a complete description refer to the source at [22]. The *Glycerol-phosphocholine-choline* and the *Ethanolamine* both deserve a particular comment, given that they show an interesting behavior in appearing in the two parts of the LSTE dataset, the Long and the Short times of echo. Looking for common metabolites with [18] (previously discussed in literature review) the following were found: Alanine, Myo-Inositol, Taurine, Choline, Glutamate and Glutamine.

Table 3: Metabolic interpretation in best models. For reading purposes the first group on each metabolite labeled. Prefix *L*, *S* signal which part belong to and all values are ppm expressed.

Metabolite	Biological interpretation
Glycerol-phosphocholine-choline	An end product of membrane phospholipid degradation and increased concentrations have been associated with cerebral ischemia, seizures and traumatic brain injury. {L3.66 S3.66}
Ethanolamine	Increased levels of this metabolite has been observed in ischemic brain tissue of rats and gerbils. {L3.81 S3.81}
Glutathione-glutamate	An anti-oxidant, essential for maintaining normal red-cell structure. Altered levels have been reported in Parkinsons's disease and other neurodegenerative diseases. {L2.18}
Alanine	A nonessential amino acid that has been observed in increased levels in meningiomas. {L1.55}
Threonine	A large neutral amino acid essential to the diet. {S4.19 S1.32}
Valine	An essential amino acid necessary for protein synthesis observed in brain abscesses. {S2.25 S1.04}
Phenylalanine	An aromatic amino acid that presents elevated readings in phenylketonuria, an abnormal phenylalanine metabolization. {L3.11 L3.07}
Glutathione-cysteine	See Glutathione-glutamate. {L2.98 L2.90}
Aspartate	An excitatory amino acid that performs as a neurotoxin in elevated concentrations [23]. {L2.75}
NAA-Aspartate	A free amino acid whose function is poorly understood, but is is commonly believed to provide a marker of neuronal density. {L2.69}
GABA	A primary inhibitory neurotransmitter whose altered concentrations are associated with neurological disorders. {L2.29 L1.86 S2.29}
Myo-inositol	Its function is not enough understood, although it is believed to be a requirement in cell growth. Altered levels have been linked with Alzheimer's disease, hepatic encephalopathy and brain injury. {S3.53}
Choline	A combination of multiple metabolites and is elevated in all brain tumors. It is required for the synthesis of neurotransmitters constituents of membranes. {S3.49}
Not identified	{L0.83 L0.62 S1.13 S0.70 S0.66}.

6 Conclusions

A feature selection algorithm has been introduced as a strategy to select subsets of spectral points from ^{1}H-MRS spectral data of brain tumors. The proposed algorithm takes advantage of the differential presence of certain metabolites that could allow to identify a specific tumor. It also accounts for possible redundancies introduced in the selected subsets of spectral points that could be derived from this approach. The final model obtained is considerable competitive in terms of accuracy, complexity of the algorithmic process needed to obtain it, and medical interpretability with respect to other solutions in the literature.

In this vein, it should be noted that, although a "best" subset of spectral points could certainly exist to solve the task at hand, it is extremely unlikely that it is found by a search process, for two reasons. The first reason is an algorithmic one, given the exponential size of the set of all possible solutions. The second reason has to do with statistical significance (all computations with finite samples are uncertain and, to some extent, unreliable) and to model assessment (the classifiers are prone to overfit small datasets). This is the reason why we complement the solution with the interpretation and visualization parts, although the expertise provided by radiologists and other clinicians is invaluable for a complete evaluation.

This study has also confirmed that the LSTE combination renders better subsets in classification accuracy terms than the other two datasets alone. Also, the results suggest that linear models are among the best suited for the task, but only after a dimensionality reduction process. In addition, most of the identified metabolites are positively defined by the medical literature and some concordances are found with successful recent machine learning works.

Acknowledgments

This work was supported by the Spanish MICINN under grant TIN2009-13895-C02-01. Authors acknowledge the former INTERPRET European project partners. Data

providers: Dr. C. Majós (IDI), Dr. À. Moreno-Torres (CDP), Dr. F.A. Howe and Prof. J. Griffiths (SGUL), Prof. A. Heerschap (RU), Prof. L Stefanczyk and Dr. J. Fortuniak (MUL), and Dr. J. Calvar (FLENI); data curators: Drs. Julià-Sapé, Candiota and Olier, Ms. Delgado, Ms. Martín and Mr. Pérez (GABRMN-UAB). Prof. C. Arús (GABRMN coordinator).

References

[1] A. Zamani, Minimal invasive Neurosurgery, Humana Press, 2005, Ch. Proton MR Spectroscopy, pp. 75–86.

[2] N. Sibtain, The clinical value of proton magnetic resonance spectroscopy in adult brain tumours, Clinical Radiology 62 (2007) 109–119.

[3] H. Bruhn, et. al., Noninvasive differentiation of tumors with use of localized h-1 mr spectroscopy in vivo: initial experience in patients with cerebral tumors, Radiology 172 (1989) 541–548.

[4] J. Hansen, et. al., ^{1}h-mr spectroscopy of the brain: Absolute quantification of metabolites, Radiology 246 (2) (2006) 318–332.

[5] A. Tate, et. al., Development of a decision support system for diagnosis and grading of brain tumours using in vivo magnetic resonance single voxel spectra, NMR in Biomedicine 19 (2006) 411–434.

[6] J. Garcia, et. al., On the use of long te and short te sv mr. spectroscopy to improve the automatic brain. tumor diagnosis., Tech. rep., In `ftp://ftp.esat.kuleuven.ac.be/pub/SISTA/ida/reports/07-55.pdf` (2007).

[7] A. Vellido, et. al., Outlier exploration and diagnostic classification of a multi-centre ^{1}h-mrs brain tumour database, Neurocomputing 72 (2009) 3085–3097.

[8] J. Usenius, et al., Automated classification of human brain tumors by neural network analysis using in vivo 1h magnetic resonance spectroscopic metabolite phenotypes., Neuroreport 7 (10) (1996) 1597–1600.

[9] M. Ala-Korpela, et al., Artificial neural network analysis of 1h nuclear magnetic resonance spectroscopic data from human plasma., Neurocumputing 13-15 (2009) 3085–3097.

[10] C. Majos, et. al., Brain tumor classification by proton mr spectroscopy: Comparison of diagnostic accuracy at short and long te, American Journal of Neuroradiology 25 (2004) 1696–1704.

[11] A. Devos, Quantification and classification of mrs data and applications to brain tumour recognition, Ph.D. thesis, Katholieke Univ. Leuven (2005).

[12] L. Lukas, et. al., Brain tumor classification based on long echo proton mrs signals, Artificial Intelligence in Medicine 31 (2004) 73–89.

[13] Y. Huang, P. Lisboa, W. El-Deredy, Tumour grading from magnetic resonance spectroscopy: a comparison fo feature extraction with variable selection, Statistics in medicine 22 (2003) 147–164.

[14] A. Nikulin, et. al., Near-optimal region selection for feature space reduction: novel preprocessing methods for classifying mr spectra, NMR in Biomedicine 11 (1998) 209–216.

[15] J. Luts, et. al., A combined mri and mrsi based multiclass system from brain tumour recognition using ls-svms with class probabilities and feature selection, Artificial Ingelligence in Medicine 40 (2007) 87–102.

[16] F. González, et. al., Feature and model selection with discriminatory visualization for diagnostic classification of brain tumors, Neurocomputing 73 (2010) 622–632.

[17] E. Romero, et. al., Feature selection with single-layer perceptrons for a multicentre ^{1}h-mrs brain tumour database, in: IWANN (1), 2009, pp. 1013–1020.

[18] P. Lisboa, et. al., Classification, dimensionality reduction, and maximally discriminatory visualization of a multicentre 1h-mrs database of brain tumors, in: ICMLA '08: Proceedings of the 2008 Seventh International Conference on Machine Learning and Applications, IEEE Computer Society, 2008, pp. 613–618.

[19] M. Castillo, L. Kwock, S. Mukherji, Clinical applications of proton mr spectroscopy, AJNR 17 (1996) 1–15.

[20] INTERPRET, International network for pattern recognition of tumours using magnetic resonance project, `http://azizu.uab.es/INTERPRET` (2002).

[21] C. Ladroue, Pattern recognition techniques for the study of magnetic resonance spectra of brain tumours, Ph.D. thesis, St. George's Hospital Medical School (2003).

[22] V. Govindaraju, K. Young, A. Maudsley, Proton nmr chemical shifts and coupling constants for brain metabolites, NMR in Biomedicine 13 (3) (2000) 129–153.

[23] A. Farooqui, W. Ong, L. Horrocks, Glutamate and Aspartate in Brain, Springer New York, 2008.

[24] P. Lisboa, et. al., Cluster based visualisation with scatter matrices, Pattern Recognition Letters 29 (13) (2008) 1814–1823.